Journal of Nuclear Materials 392 (2009) 28–34

Contents lists available at ScienceDirect

Journal of Nuclear Materials

journal homepage: www.elsevier.com/locate/jnucmat

Predicting the probability for fission gas resolution into uranium dioxide

David C. Parfitt, Robin W. Grimes *

Department of Materials, Imperial College London, London SW7 2AZ, UK

ARTICLE INFO

Article history:
Received 17 November 2008
Accepted 11 March 2009

ABSTRACT

Classical molecular dynamics simulations, using a set of previously established pair potentials, have been used to predict the minimum energy needed for krypton and xenon atoms to be resolved into uranium dioxide across a perfect (1 1 1) surface. The absolute minimum energy, E_{min}, is 53 eV for krypton and 56 eV for xenon atoms, significantly less than the 300 eV value often assumed in fuel modelling as the minimum energy required for gas resolution. The present values are, however, still sufficient to preclude thermal resolution at normal reactor temperatures. The discrepancies between the present and previous resolution energies are due to the significant variation in probabilities of absorption at different impact points on the crystal surface; we have mapped out the probability distribution for various impact sites across the crystal surface. The value of 300 eV corresponds to an 85% chance of resolution.

1. Introduction

Fission gas atoms such as krypton (Kr) and xenon (Xe) are produced in uranium dioxide as a part of the fission process either directly or subsequently from other decay products. Once formed, the high heat of solution of these species in UO_2 drives their precipitation into microscopic bubbles of gas within the fuel matrix [1–6]. As the fuel ages, these fission gas bubbles accumulate in the interior of fuel grains and in larger inter-granular bubbles [7–12]. The presence of the bubbles leads to changes in the fuel microstructure [2,13–20] and a corresponding degradation of the material properties of the fuel [13,14,17–23]. Additionally, at high burnup, the linkage of inter-granular bubbles [8,21–30] leads to the release of fission gas to the fuel-clad gap. This degrades the thermal contact between the fuel and cladding.

Neither Kr or Xe are soluble in UO_2 [31–37]. This provides the driving force to move these species from the lattice into bubbles or to escape from the fuel entirely. In reality, however, the constant generation of fission gasses in the lattice, the thermal diffusion of Xe and Kr at reactor temperatures [32,37,38] and dynamic effects such as radiation cascades occurring within the fuel [1,14,25,38–44] will all contribute to produce a gas atom population that is distributed between sites within the crystalline lattice and gas bubbles of varying sizes. The bubbles therefore act as reservoirs, absorbing gas atoms from the lattice and returning them through processes such as radiation-enhanced resolution [1,14,25,38–45]. The relative rates of these processes determines the overall size and density of these bubbles.

In this paper, we examine the activation energy necessary to return Kr and Xe atoms from the bubbles back into the crystalline lattice. In a real material this may occur through two distinct mechanisms. The first is thermal resolution, in which a single atom in a gas bubble collides with the bubble surface with a kinetic energy, acquired through thermal excitations, sufficient to place it back into the crystal lattice. The second mechanism is radiation-enhanced resolution [1,14,25,38–45]. In this case, gas atoms recoil from collisions with energetic fission fragments traversing the bubble–crystal interface and may be promoted deep into the crystal lattice. Though very different in physical origin, these two mechanisms may be conveniently linked through a single parameter, E_{min}. This has been described as the minimum energy needed for a single gas atom to overcome the surface tension of the bubble and penetrate 'sufficiently far' into the crystal lattice such that re-precipitation does not trivially occur [44].

Our simulations consider Kr and Xe atoms impacting upon a (1 1 1) O^{2-} terminated defect-free UO_2-surface. We have considered impacts over a finely spaced grid of points of the primitive surface cell. These simulations will predict a range of minimum energy values, E_{min}, and thereby obtain relationships for E_{min} as a function of entry position.

We have not considered crystalline surfaces other than the lowest energy, that is the most stable, {1 1 1} terminated planes [46], nor any defective or rough surface configurations. This is an important simplification: in a previous paper [47] we have already discussed the role of surface damage in providing a pathway to accommodate gas resolution into the lattice. Here, however we reduce the complexity of the model by considering solution into an initially undamaged surface. Therefore, in this first study we concentrate on identifying how impact energy and impact position on the surface influences the depth to which gas atoms are incorporated into the lattice.

The remainder of this paper is organised as follows. In the next section we discuss briefly some of the most relevant experimental

* Corresponding author. Tel.: +44 20 7594 6730.
E-mail address: r.grimes@imperial.ac.uk (R.W. Grimes).

0022-3115/$ - see front matter © 2009 Elsevier B.V. All rights reserved.
doi:10.1016/j.jnucmat.2009.03.046

studies and the empirical resolution models that have been developed to explain them. In Section 3 we define the interatomic potential parameters we are using together with the impact geometry for the simulations. The results section summarises the main findings of this paper. We present examples of both the general form of the cascade damage within the crystal and specific final defect configurations that may arise. We also establish E_{min} for a range of impact positions for both Kr and Xe.

Section 5 examines the results from this paper in terms of simple classical models of atomic interactions in order to interpret aspects of the functional form of the resolution probability. We conclude in Section 6 with some general remarks on the comparison of these atomic scale results to previous empirical models and experimental observations of gas resolution.

2. Gas resolution models

There is a wealth of previous studies that have examined both the experimental and theoretical behaviour of fission gas bubbles in UO_2. A recent series of reviews [48,49] has considered the resolution of fission gas from intra- and inter-granular bubbles [49] and the impact these models have upon the total levels of gas resolution. We summarise here the relevant literature concentrating on the overall physical size and shape of fission gas bubbles. We also consider some of the empirical models that have been developed to explain the various resolution rates and the parameters within these models which are ill-defined or unknown from empirical data but may be within the scope of atomic scale simulations.

2.1. Physical properties of intra-granular fission gas bubbles

The concentration of fission gasses in UO_2 varies from zero in an un-irradiated fuel to a few percent of the metal atom concentration in a material close to the end of its useful life in a reactor [25,29,50]. The majority of this gas is held, for all but the smallest gas concentrations, in gas bubbles either distributed through the UO_2 matrix or at grain boundaries. The bubbles vary in size from nanometers up to several microns [4,27,51,52].

The resultant pressure in the bubbles is the sum of the external stress on the UO_2 material and surface tension of the bubble void. It is rather poorly defined in resolution models partly because of the failure of a traditional gas equation of state in the very small, high pressure regime but also because the bubbles may be in states far from equilibrium, because of rapid changes in temperature or a local deficit of lattice vacancies from which to grow [9,23,27,53]. Typically, however, the smallest bubbles are assumed to have densities comparable to that of solid xenon [54], larger bubbles (where the gas-law equation of states are more applicable) have correspondingly lower densities and pressures.

2.2. Current resolution models

Many theoretical models have evolved to explain the levels of resolution from gas bubbles in UO_2. Common to almost all is the assumption that thermal resolution plays little role in returning gas atoms to the UO_2 lattice. The dominant mechanism of resolution is one linked to the interaction of the gas in the bubbles with fission fragments passing through the crystal matrix. Two possible mechanisms are proposed: heterogeneous and homogeneous.

In the heterogeneous model, bubbles are almost completely destroyed by the passage of a fission fragment in the vicinity of the bubble. The destruction of the bubble occurs through either the vapourisation of the dense gas due to the passing pressure wave or to the trapping of gas atoms in material thrown from one side of the bubble to the other [49]. These mechanisms require modelling of the entire interaction of the bubble with the fission spike, the ballistic part of which has an energy of several million electron volts, and is computationally rather beyond current resources.

The second mechanism, homogeneous resolution, relies upon individual gas atoms being ejected from the bubble mass through collisions with fission fragments or recoil uranium atoms, that are traversing the bubble. The kinetic energy acquired through such collisions can range up to the maximum ballistic energy of a fission fragment, which is several million electron volts. For resolution to be achieved a gas atom must acquire energy above the critical value E_{min}.

The resolution parameter, b, for a bubble is defined as the rate of fission gas resolution per unit time which, for the homogeneous mechanism, corresponds to the inverse of the mean time a fission gas atom spends in the bubble. As a function of the fission fragment energy, E_{ff}, and the kinetic energy transferred to the resolved atom E, the rate of resolution can be written as the double integral over the possible recoil energies E, and the possible fission fragment energies E_{ff} upto the maximum E_{ff}^{max},

$$b = \int_{E_{min}}^{E_{ff}^{max}} \phi(E_{ff}) \mathrm{d}E_{ff} \int_{E_{min}}^{E_{ff}} \upsilon(E) \sigma(E_{ff}, E) \mathrm{d}E, \quad (1)$$

where $\phi(E_{ff})$ is the spectrum of initial fission fragments, $\sigma(E_{ff}, E)$ is the differential cross-section for transfer of energy E to a gas atom from a fission fragment of initial energy E_{ff} and υ is the number of fission gas atoms generated as a result of the initial transfer of energy.

The initial formulation and estimate of the rate of homogeneous resolution was made in a paper by Nelson [44], taking the minimum energy E_{min} for resolution to be 300 eV. Below this values the probability of resolution is assumed to be zero, above E_{min} the gas atom will achieve resolution with a probability of 100%. In this paper we focus on an improved estimate and model for the parameter E_{min}.

3. Methodology

Classical molecular dynamics simulations have been used in this study to examine the behaviour of gas atoms impacting the (1 1 1) surface of UO_2. The molecular dynamics code DLPOLY version 3.02 was used [55,56]. There have been a number of empirical pair potentials developed to model the behaviour of cascade damage in UO_2 [57–62], here we use a set that has previously been used to model the interaction of uranium and oxygen ions and the Kr and Xe atoms [32,33,63].

The simulations reported here require large numbers of calculations for a range of initial impact parameters, each simulation must necessarily be computationally efficient. We made full use of the variable timestep available in DLPOLY to scale the integration timestep at each simulation frame so that the ions were only able to move between a certain preset range of distances. Such a method allows the efficient sampling of the dynamics of the system during both the energetic ballistic region (where a short timestep of a fraction of a femtosecond may be necessary) and the longer equilibration period (where the dynamics are much slower and a short timestep would be computationally wastefull).

To create the initial simulation configuration we began with the experimentally reported fluorite unitcell of UO_2. We are interested in the (1 1 1) surface of this structure and so we took a $10 \times 10 \times 5$ supercell of the UO_2 structure in its hexagonal setting to create a 4500 atom initial configuration with dimensions $a \equiv b = 3.8679$ nm, $c = 4.7372$ nm and $a \cdot b = |a||b| \cos 120^\circ$. This configuration was relaxed in the micro-canonical ensemble with periodic boundary conditions for 10000 timesteps ($\sim$50 ps) at a temperature of 300 K to allow the potential and kinetic degrees of motion to come into equilibrium. A Nose–Hoover thermostat with a relaxation time of 0.5 ps was used to maintain the kinetic temperature during this time.

Following equilibration of the bulk material, the surfaces were formed by cleaving a plane of adjacent oxygen ions perpendicular to the *c* direction ([1 1 1] in the old cubic setting), this surface was charge neutral and type II in the nomenclature of Tasker [64]. The (1 1 1) surface has previously been shown to exhibit the lowest surface energy and dominates the equilibrium crystal morphologies [46,65]. The cleaved material was separated by a gap of 3.5 nm along the *c*-axis and periodic conditions re-applied such that the configuration now consisted of periodic blocks of width $c \sim 4.7$ nm separated by a vacuum gap of 3.5 nm. This configuration was again allowed to relax for a total of 10000 timesteps.

To begin the cascades a single Kr or Xe atom was inserted a distance 1.0 nm from one of the surfaces; as the gas atom has zero charge and the van der Waals forces are small at this distance from the surface, the net change in potential energy in introducing this atom is negligible. The atom was given a kinetic energy *E* with a momentum directed towards the surface of the crystal.

4. Results

Fig. 1 shows the trajectory of a 500 eV Kr atom impinging upon the (1 1 1) surface. Over the 20 ps of the simulation the gas atom enters the lattice, creates significant levels of disorder and finally comes to rest at a lattice site, while the remainder of the disorder dissipates around it. Labels a–d in Fig. 1 indicate important events occurring during a typical cascade. In chronological order these are,

(a) The atom begins its path 1.0 nm from the crystalline surface. The initial trajectory is therefore straight and the atom enters the lattice at a point **r** on the surface of the crystal.
(b) The mass of the Kr atom is significantly greater than the mass of the oxygen ions and less than the mass of the uranium ions, thus the path followed is dominated by collisions with uranium ions.
(c) The significant difference in mass also dominates the structure of the secondary cascades. Kr atoms can knock both uranium and oxygen ions off of their lattice sites; the uranium ions can go on to cause significant damage to both the uranium and oxygen sublattices, the oxygen ions, however, are only effective in damaging their own sublattice.
(d) Once it has lost sufficient kinetic energy the Kr atom becomes trapped in either an interstitial or, as here, a vacant uranium site, although in our simulations either trap site was often surrounded by significant residual disorder on the oxygen sublattice.

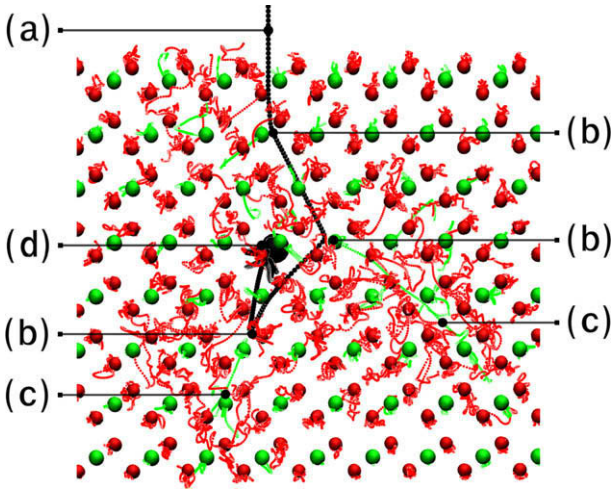

Fig. 1. Example of the trajectories seen in a typical cascade with a krypton atoms impacting at normal incidence to the surface. The positions of uranium ions are plotted in green, oxygen in red and the krypton atom in black. Large points show the initial positions of the uranium and oxygen atoms at the point of cascade initiation and the final position of the krypton atom after approximately 3 ps of simulation time. Smaller points show the evolution of the atomic positions sampled every 100 timesteps. Labels (a–d) refer to features discussed in the text. (For interpretation of the references in colour in this figure legend, the reader is referred to the web version of this article.)

We will consider three points that relate directly to the case of surface incorporation of Kr and Xe. First, we examine the minimum impact energy needed to create shallow surface defects and identify any differences between the gas atom species. Second, we consider the depth in the lattice a gas atom may penetrate as a function of the impact energy. Third, we examine the final defect configurations formed by the impacting gas atoms. This is to assess whether the structures that form are similar to those predicted to occur in the bulk [32,33] and also to establish which very shallow defect configurations are stable on the short timescales considered here.

4.1. Kr and Xe defect structures

Fig. 2 shows the results for Kr and Xe atoms with a range of kinetic energies impacting at normal incidence upon randomly selected positions over the (1 1 1) surface primitive-cell. Atoms that collided with the surface and re-bound are not plotted in this figure. The impact depth depends upon both the energy and impact position, so in Fig. 2 there are multiple possible penetration positions corresponding to the same kinetic energy. However, these randomly selected values demonstrate the range of behaviour apparent as a function of initial kinetic energy. Clearly, below a certain energy, approximately 50 eV for both Kr and Xe, no resolution occurs and the gas atoms are returned to the vacuum. Above this energy the atoms can form stable defects within the crystal, although the positions of these species are confined to certain depths corresponding to crystallographic positions within the bulk. Each depth has, in turn, a minimum energy needed to incorporate a gas atom, and both the depths and corresponding minimum energies are marked in Fig. 2.

In Fig. 3, we examine the form of two specific defect structures obtained after several picoseconds relaxation time. These two structures correspond to examples of the shallowest and second-shallowest Kr atom positions observed in the simulations: Fig. 3(a) shows the Kr atom located in the interstitial site immediately below the surface and Fig. 3(b) shows the accommodation of the Kr atom on a site previously occupied by a U^{4+} ion in the second layer of atoms. We did not observe Kr or Xe atoms substituting in the shallowest layer of U^{4+} ions – this site provides a route for the gas atoms back into the vacuum with a negligible activation energy, and is therefore not stable even on the short timescales considered here.

The trajectories plotted in Fig. 3 also help to explain the differing penetration depths shown in Fig. 2. In order to create a stable defect structure to accommodate a gas atom (at either an interstitial or substitutional site), the Kr or Xe atoms must displace one or more ions from their lattice sites in each layer through which they pass (in order to create a pathway to the next layer). Such a pathway may be formed by successive displacements of O^{2-} ions (in which case the atom can only occupy interstitial sites), alternatively pathways may involve displaced U^{4+} ions, in which case the atom *may* end up at U^{4+} substitutional sites. The threshold energy for ion displacements in UO_2 have been calculated previously [66,59] and depend strongly upon the ion species, direction of displacement and the functional form of the interatomic potential used. We note, however, that in general (i.e. irrespective of

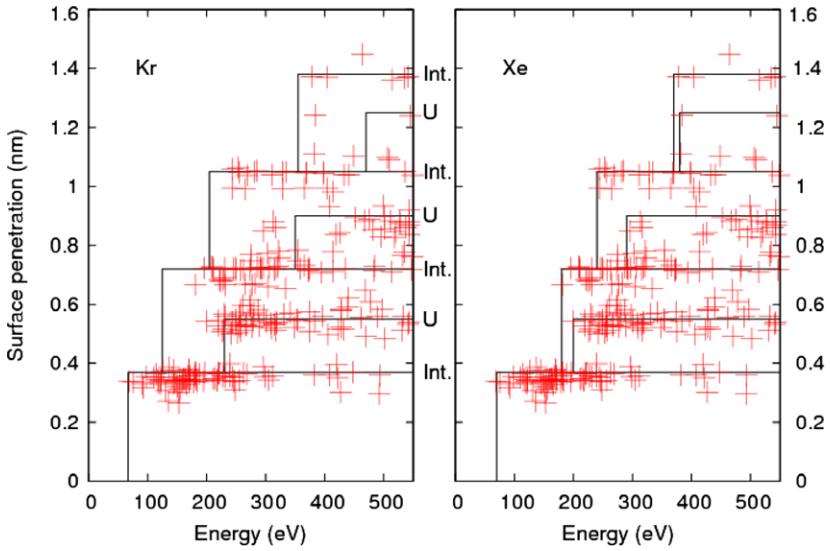

Fig. 2. Penetration of Kr and Xe atoms into the surface for energies ranging from 50 to 600 eV. Each individual point represents a single simulation with an impact point randomly chosen to lie on the crystalline surface primitive-cell and as such the data are effectively averaged over the entire surface of the crystal. Solid labeled lines represent the depth of the interstitial (1/2,1/2,1/2) and uranium ion (0,0,0) sites in the crystalline bulk, additional solid lines represent the lowest energy at which each class of defect was observed.

direction) O^{2-} threshold energies are lower than U^{4+}, and also that the transfer of energy from the gas atom to the lattice ions will depend upon the ratio of their masses. Thus, Kr and Xe atoms will be able to displace O^{2-} ions more easily than they will U^{4+} ions, and Xe atoms will be better at displacing U^{4+} ions than will Kr. A Kr atom with insufficient energy to displace a U^{4+} ion may, nevertheless, proceed into the lattice via a set of steps displacing only O^{2-} ions and loosing at least 60 eV for each displacement. This gives rise to the staircase-like structure observed in Fig. 2 with gas atoms residing in successively deeper interstitial sites. However, for the Kr atom to penetrate beyond three layers it will also have had sufficient energy to displace a U^{4+} ion and so this alternative accommodation mechanism may come into operation so that the Kr atom may then occupy a U^{4+} substituted site. This trend is exhibited in Fig. 2 so that for Kr, the minimum energy to create a U^{4+} substituted site is $\sim$ 230 eV and for Xe $\sim$ 205 eV.

A wide variety of final defect structures were produced due to the impact of gas atoms upon the surface. For example in Fig. 3(a) the interstitial Kr atom is surrounded by clearly distorted but nonetheless non-defective UO_2. Conversely, in Fig. 3(b) the U^{4+} substituted Kr atom is stabilised by a single adjacent O^{2-} vacancy. We did not, however, observe Kr or Xe atoms occupying vacant O^{2-} sites, despite the considerable displacement damage that this sublattice experiences. In bulk UO_2, defect energies have previously been calculated for Kr and Xe in several defect configurations, and a preference is shown for accommodation in a neutral trivacancy (a uranium vacancy accompanied by two oxygen vacancies). However, the second greatest preference is for accommodation at a divacancy (a uranium vacancy adjacent a single oxygen vacancy) [32] i.e. as observed in Fig. 3(b). Significantly, accommodation of gas atoms at an O^{2-} vacancy was predicted to be particularly unfavorable [32]. Why then, given the rapid mobility of the O^{2-} ions on their sub lattice, do we not always observe the neutral trivacancy? There are two related reasons: Firstly to form an isolated trivacancy, it is necessary to expel one U^{4+} and two O^{2-} ions to the surface. However, we have relaxed our structure over only a few picoseconds and therefore have not reached this thermal equilibrium. Secondly, once the kinetic energy from the impact has dissipated the migration barriers in UO_2 are correspondingly long compared to these time scales. Consequently the defects produced here often remain in close proximity to one another and will compete for available O^{2-} defects. For example, in Fig. 3(b), the O^{2-} ion that would be removed to form the second oxygen vacancy of the trivacancy is unlikely to move far from the U^{4+} interstitial.

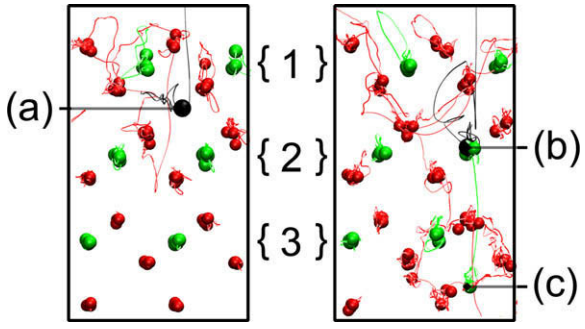

Fig. 3. Example cascades showing creation of interstitial (left) and U^{4+}-substituted (right) Kr defects. Similarly to Fig. 1, U^{4+} ions are plotted in green, O^{2-} ions are plotted in red and the Kr atom in black. Large spheres show the final positions of the atoms after the end of the simulation, continuous ribbons connect together the trajectories followed by the atoms during the simulation. Numerical labels refer to successive layers of U^{4+} and O^{2-} ions from the surface downward. Also labeled are (a) a Kr atom in the first interstitial site, (b) a Kr atom substituting onto a U^{4+} site, and (c) the formation of a U^{4+} interstitial ion. (For interpretation of the references in colour in this figure legend, the reader is referred to the web version of this article.)

Finally, a common way of simulating ion implantation is to consider SRIM type calculations [67]. These are typically used to calculate depths for far higher implantation energies than those considered here, nonetheless we can compare the results of our simulations with the depth penetration at only very low energies predicted by SRIM. Although very different in computational approach SRIM calculations predict typical ion implantation depths in UO_2 of 1.3 nm for an implantation energy of 500 eV, in very close agreement with the range of values shown in Fig. 3.

4.2. Minimum energy for normal resolution

Due to differences in the way the gas atoms are scattered by the surface ions, each impact position upon the primitive surface cell

will have a characteristic minimum energy to place a gas atom into a shallow, but stable defect position. In order to calculate this energy across the range of different impact positions we have adopted the following approach.

(a) A 13 × 13 evenly spaced rhombohedral grid of positions was created across the primitive unit cell from fractional coordinates of 0–1 inclusive (i.e. 12 unique positions and a 13th set that was calculated to check for periodic conditions at the edge of the cell). Simulations were run for 2500 timesteps at each of these positions with an initial kinetic energy for the gas atom of 200 eV.
(b) For each of these simulations the gas atom trajectory was analysed to determine whether it had been repelled by the surface or been incorporated into the crystal.
(c) If the atom has been repelled, the initial kinetic energy was increased, if it has not then the kinetic energy was decreased and the simulation repeated.
(d) Steps (b) and (c) were repeated until the value had converged to within 1 eV.
(e) The grid of surface energy values was then interpolated using a quadratic fit to the nearest three neighbouring points to produce a continuous value of E_{min} as a function of impact position.

Fig. 4 shows details of the minimum energy surface for both Kr and Xe atoms. The dominant feature of these plots is the strong maximum around $(\frac{1}{3},\frac{2}{3})$ corresponding to the position of the topmost U^{4+} ion in the surface. For a direct head-on collision of a Kr/Xe atom with a higher-mass U^{4+} ion the recoil will always reflect the atom away from the crystal surface no matter how high the energy.

No significant maxima exist over the two lower U^{4+} sites suggesting that for these impacts there exist shallow defect positions able to accommodate the impinging gas atom without recoil. To reach these positions, Kr or Xe atoms must displace O^{2-} ions and thus there is a minimum energy, however, it is not as great as that required to displace a U^{4+} lattice ion.

Using the data in Fig. 4 it is now possible to calculate an overall probability of normal resolution as a function of initial impact energy. To achieve this the primitive surface cells are integrated along the energy axis to calculate, for a given energy, the fraction of total UO_2 (1 1 1) surface that the impacting gas atom can penetrate into. The results of these calculations, for Kr and Xe, are plotted in Fig. 5. We are able to extract from this figure an effective E_{min} of 53.0 eV for Kr and 56.4 eV for Xe atoms though the probability of resolution is very small for values less than 80 eV. We define therefore a more representative measure, $E_{1/2}$, as the energy at which resolution exceeds 50% probability. This corresponds to an energy of 130 eV for Kr and 152 eV for Xe atoms. The value of E_{min} used previously, 300 eV, corresponds to a probability of ~85% for resolution of gas, and in this context 300 eV seems a sensible value to have employed.

5. Discussion

We now consider the simulations in terms of simple classical models of atom–atom interactions. This helps promote the transferability of the work to other systems. It also allows us to address the issue of whether the resolution probabilities (Fig. 5), which are composed of many individual simulations, are physically sensible. Usually we would wish to compare with experimental data but this is not possible here, at least not at the necessary level of detail. There are three features of the probability function to consider: the

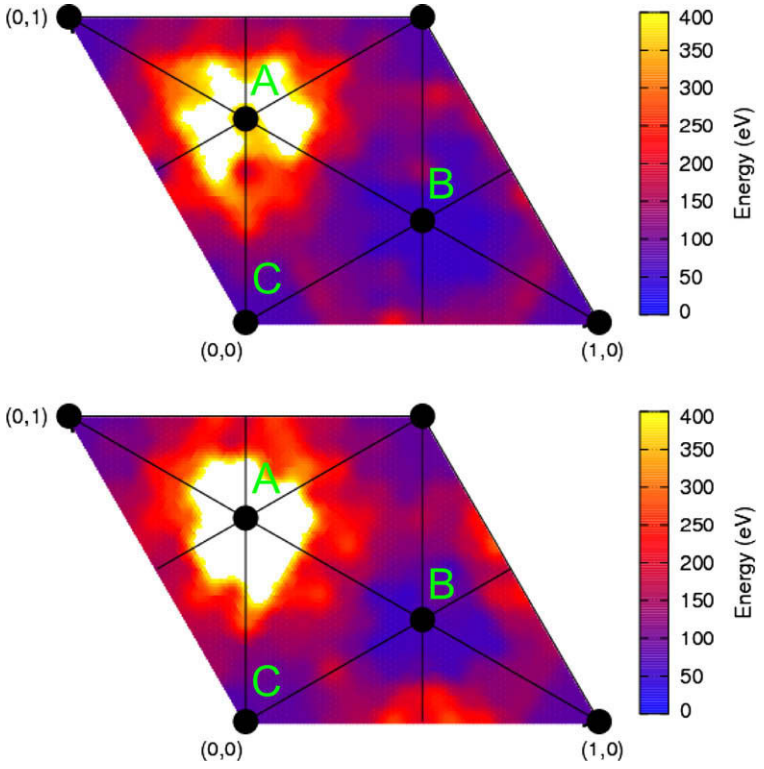

Fig. 4. Map of the minimum energy required to achieve incorporation of Kr (top) and Xe (bottom) atoms into the (1 1 1) surface of UO_2 plotted over the primitive surface cell. Colours represent calculated energies ranging from dark (low minimum energy) to light (high minimum energy). Filled circles and lines represent the network of uranium atoms beneath the surface, these are labeled A, B and C in order of depth from the surface.

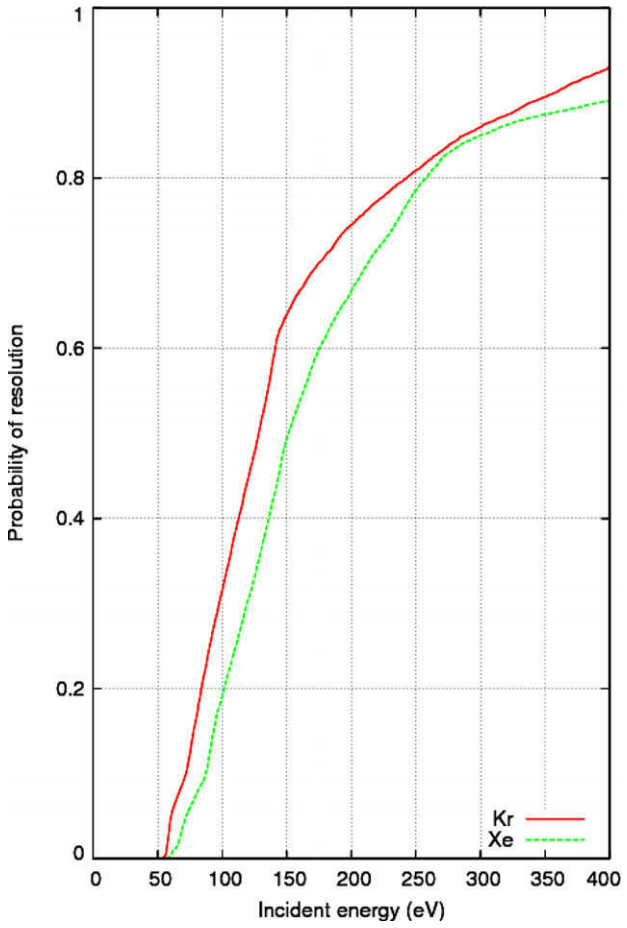

Fig. 5. Probability of resolution for Kr (solid-red) and Xe (dotted-green) atoms as a function of initial impact energy, the data are calculated from the surface-integral of the plots shown in Fig. 4. (For interpretation of the references in colour in this figure legend, the reader is referred to the web version of this article.)

low energy threshold value, the differences between the Kr and Xe probability functions and the limiting high energy behaviour.

The classical model we use assumes the geometry shown in Fig. 6; here an atom approaches with momentum **p** a second stationary ion. The atoms are modelled as spheres where the sum of the two radii is σ and the shortest distance separating the centre of the stationary ion and the projection of the initial momentum (i.e. the impact parameter) is d.

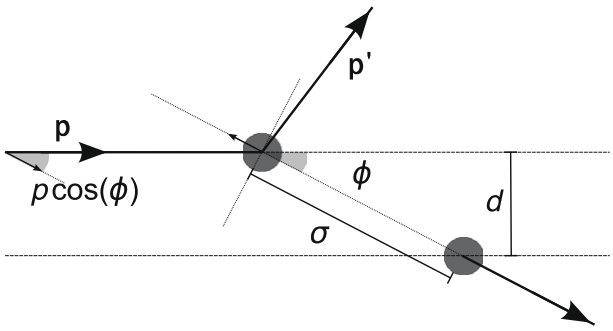

Fig. 6. Impact geometry for a collision between a gas atom and lattice ion assuming a hard-sphere model. The gas atom approaches an initially stationary ion with momentum **p**, the collision occurs at a distance σ transferring an impulse along the radial direction separating the centres of the two spheres. The gas atom leaves with momentum **p**′.

During the collision, which we consider initially to be hard and elastic, a momentum $\Delta\mathbf{p}$ is transferred along the radial line between the two atom centres. Conservation of momentum along this radial direction leads to the magnitude of change of momentum of each atom being,

$$|\Delta p| = \frac{2|p|\cos(\phi)}{1 + m_{\text{gas}}/m_{\text{ion}}}, \tag{2}$$

where ϕ is the scattering angle through which the gas atom is reflected (shown in Fig. 6) and is defined from geometric relations as $\sin(\phi) = d/\sigma$. m_{gas} and m_{ion} are the masses of the incident gas atom and lattice ion respectively.

We may also consider the energy transferred from the gas atom to atoms within the crystal. From Eq. (2) we can write the energy transferred to the atom, ΔE, in terms of the energy of the initial gas atom E as,

$$\frac{\Delta E}{E} = \frac{4(1 - d^2/\sigma^2)}{(1 + m_{\text{gas}}/m_{\text{ion}})^2} \cdot \frac{m_{\text{gas}}}{m_{\text{ion}}}. \tag{3}$$

5.1. Threshold behaviour

Our simulations suggest that for finite levels of resolution it is necessary for the Xe or Kr atoms to displace ions from their lattice sites if they are to pass deeper into the lattice. Furthermore, the lowest energy resolution process requires the displacement of a single O^{2-} surface ion. The minimum threshold energies needed to create lattice defects (i.e. to displace an O^{2-} or a U^{4+} ion from its crystalline lattice site) has been calculated in UO_2 [66] and is a function of the high energy interaction potential, ion location and direction of ion recoil.

We have recalculated these threshold energies specifically for the potentials used here. The values are of 27.4 eV and 72.5 eV for O^{2-} and U^{4+} ions respectively, and are similar those previously calculated [66]. These are comparable with the minimum value of E_{min} suggested by our simulations, that is, 53.0 eV (Kr) and 56.4 eV (Xe). The small differences arise from the transfer of energy from the more massive gas atom to the O^{2-} ion and that the recoil direction in our calculations is not aligned with the direction of minimum energy.

5.2. Relationship between Xe and Kr probability functions

Although we may envisage a single collision geometry producing the very lowest energy resolution, at higher energies there are a range of contributing processes. It is, however, evident from Fig. 4 that the gross behaviour is relatively simple. That is, after the threshold energy is reached the probability of resolution increases rapidly with energy. Then, once a probability of around 2/3 is reached, the increase becomes slower.

Although we cannot identify the exact form of the resolution probability, the same processes occur for both types of gas atom. In particular, the resolution process consists of a series of energy transfers (collisions) with lattice ions (which may or may not cause displacements). However, according to Eq. (3) individual processes will transfer a proportion of energy, which will depend on whether that atom is Kr or Xe, therefore we can calculate the ratio according to the following equation,

$$\frac{E_{\text{Xe}}}{E_{\text{Kr}}} = \left(\frac{1 + m_{\text{Xe}}/m_{\text{ion}}}{1 + m_{\text{Kr}}/m_{\text{ion}}}\right)^2 \cdot \frac{m_{\text{Kr}}}{m_{\text{Xe}}} \cdot \frac{1 - d^2/\sigma_{Kr}^2}{1 - d^2/\sigma_{Xe}^2}, \tag{4}$$

where E_{Kr}, E_{Xe} and m_{Kr}, m_{Kr} are the energies and masses of the Kr and Xe atoms and we have retained the distinction between the effective radii of Kr (σ_{Kr}) and Xe (σ_{Xe}). In this case we make the simplification that for these intermediate energies the differences

between radii are negligible and take $\sigma_{Xe} \equiv \sigma_{Kr}$ we obtain the ratio between the two energies to be,

$$E_{Kr} = 1.194 \times E_{Xe}. \quad (5)$$

That is, to produce the equivalent displacive effect in the lattice, a Kr atom must have a 19.4% larger initial kinetic energy than an equivalent impact with a Xe atom. The ratio between the resolution probability of Kr and Xe calculated from Fig. 5, between 10% and 60% probability, shows that for a Kr atom to have the same resolution probability as a Xe atom it must have 20.7% greater initial kinetic energy, in remarkably close agreement with the simple energy transfer model.

5.3. High energy behaviour

For very high energies the probability of resolution is dominated solely by the recoil from the U^{4+} ions in the shallowest surface layer. For this direct collision the probability will reach a limit determined (in the hard-sphere model) by the size of the interacting ions. Fig. 5 shows this as a flattening out of the resolution probability for both Kr and Xe atoms.

The typical interaction distance for a high energy collision can be calculated from a Ziegler–Biersack–Littmark universal potential [67] and for an energy of 300 eV is around 0.1 nm for both Kr and Xe atoms. Taking the ratio of this with the area of the primitive-cell we obtain a resolution of around 92–94%, in agreement with the high energy regime exhibited in Fig. 5.

6. Conclusions

In this paper, atomic scale simulations have been used to study the resolution of Kr and Xe atoms into the UO_2 lattice. The aims have been to (i) establish the magnitude of the absolute minimum energy of resolution for Kr and Xe atoms, (ii) investigate the relationship between the energy required for resolution and the impact position, and (iii) investigate the properties of the surface defects formed as a result of resolution.

The absolute lowest energies, E_{min}, determined from simulations for resolution are 53.0 eV and 56.4 eV for Kr and Xe respectively. More useful values for further fuel modelling, however, may be the energies required for a 50% probability of resolution, $E_{1/2}$, which are 130 eV and 150 eV for Kr and Xe atoms respectively. Prior to this work, it was assumed [44] that above 300 eV the resolution probability is unity and below this value no resolution occurs. Based on the present simulations 300 eV corresponds to an 85% probability of resolution.

The predicted overall relationship between the probability of resolution and the incident energy of a Kr or Xe atom is illustrated in Fig. 5. Above the absolute lowest energies for displacement and up to an energy of approximately 200 eV only O^{2-} ion defects are formed. Beyond 200 eV, both O^{2-} and U^{4+} defects can be formed as a result of the resolution process. Despite the compendium of individual processes from which the resolution probability relationship is constructed, crucial aspects can be explained by simple classical arguments. This provides us with confidence that this simulation-based approach to discovering such relationships is leading us in a fruitful direction, although clearly there is more to consider.

Acknowledgements

This work was carried out as part of the TSEC programme KNOO and as such we are grateful to the EPSRC for funding under grant EP/C549465/1. Calculations were performed on the Imperial College High Performance Computing Service. This research was partly supported by the European Commission through the FP7 F-BRIDGE project (Contract No. 211690).

References

[1] R.M. Cornell, J.A. Turnbull, J. Nucl. Mater. 41 (1971) 87.
[2] B.R.T. Frost, Nucl. Appl. Technol. 9 (1970) 128.
[3] P. Garcia, P. Martin, G. Carlot, E. Castelier, M. Ripert, C. Sabathier, C. Valot, F. D'acapito, J.L. Hazemann, O. Proux, V. Nassif, J. Nucl. Mater. 352 (2006) 136.
[4] K. Govers, S. Lemehov, M. Verwerft, J. Nucl. Mater. 374 (2008) 461.
[5] P. Losonen, J. Nucl. Mater. 280 (2000) 56.
[6] A.D. Whapham, Philos. Mag. 26 (1972) 399.
[7] C. Baker, J. Nucl. Mater. 66 (1977) 283.
[8] M. Charles, Ann. Chim. – Sci. Mater. 10 (1985) 415.
[9] J.H. Evans, A. Vanveen, K.T. Westerduin, J. Nucl. Mater. 195 (1992) 250.
[10] J.H. Evans, J. Nucl. Mater. 188 (1992) 222.
[11] J.H. Evans, J. Nucl. Mater. 210 (1994) 21.
[12] J.H. Evans, J. Nucl. Mater. 238 (1996) 175.
[13] H. Assmann, H. Stehle, Nucl. Eng. Des. 48 (1978) 49.
[14] C.C. Dollins, H. Ocken, J. Nucl. Mater. 45 (1972) 150.
[15] C.C. Dollins, J. Nucl. Mater. 49 (1973) 10.
[16] C.C. Dollins, J. Nucl. Mater. 60 (1976) 107.
[17] S.B. Fisher, R.J. White, P.M.A. Cook, S. Bremier, R.C. Corcoran, R. Stratton, C.T. Walker, P.K. Ivison, I.D. Palmer, J. Nucl. Mater. 306 (2002) 153.
[18] J.A. Turnbull, C.A. Friskney, J. Nucl. Mater. 71 (1978) 238.
[19] K. Une, K. Nogita, S. Kashibe, M. Imamura, J. Nucl. Mater. 188 (1992) 65.
[20] R.M. Carroll, Nucl. Safety 12 (1971) 297.
[21] M.S. Veshchunov, J. Nucl. Mater. 346 (2005) 208.
[22] C.T. Walker, P. Knappik, M. Mogensen, J. Nucl. Mater. 160 (1988) 10.
[23] R.J. White, J. Nucl. Mater. 325 (2004) 61.
[24] I.R. Brearley, D.A. Macinnes, J. Nucl. Mater. 118 (1983) 68.
[25] S. Bremier, C.T. Walker, Radiat. Eff. Def. Solids 157 (2002) 311.
[26] K. Forsberg, A.R. Massih, Modell. Simul. Mater. Sci. Eng. 15 (2007) 335.
[27] S. Kashibe, K. Une, K. Nogita, J. Nucl. Mater. 206 (1993) 22.
[28] Y.S. Kim, J. Nucl. Mater. 326 (2004) 97.
[29] Y.H. Koo, D.S. Sohn, Y.K. Yoon, J. Nucl. Mater. 209 (1994) 62.
[30] K. Une, S. Kashibe, J. Nucl. Sci. Technol. 27 (1990) 1002.
[31] H. Kleykamp, J. Nucl. Mater. 131 (1985) 221.
[32] R.G.J. Ball, R.W. Grimes, J. Chem. Soc., Faraday Trans. 86 (1990) 1257.
[33] C.R.A. Catlow, R.W. Grimes, J. Nucl. Mater. 165 (1989) 313.
[34] J.P. Crocombette, J. Nucl. Mater. 305 (2002) 29.
[35] R.W. Grimes, C.R.A. Catlow, A.M. Stoneham, J. Am. Ceram. Soc. 72 (1989) 1856.
[36] R.W. Grimes, C.R.A. Catlow, Philos. Trans. R. Soc. London, Ser. A 335 (1991) 609.
[37] J.C. Carter, E.J. Driscoll, T.S. Elleman, Phys. Stat. Solidi A 14 (1972) 673.
[38] M.S. Veshchunov, J. Nucl. Mater. 277 (2000) 67.
[39] J.A. Turnbull, R.M. Cornell, J. Nucl. Mater. 41 (1971) 156.
[40] J.A. Turnbull, J. Nucl. Mater. 38 (1971) 203.
[41] J.A. Turnbull, Radiat. Eff. Defects Solids 53 (1980) 243.
[42] J.A. Turnbull, C.A. Friskney, J.R. Findlay, F.A. Johnson, A.J. Walter, J. Nucl. Mater. 107 (1982) 168.
[43] S. Yamagishi, T. Tanifuji, J. Nucl. Mater. 59 (1976) 243.
[44] R.S. Nelson, J. Nucl. Mater. 25 (1968) 227.
[45] R. Whapham, Nucl. Appl. 2 (1966) 123.
[46] M. Abramowski, R.W. Grimes, S. Owens, J. Nucl. Mater. 275 (1999) 12.
[47] D.C. Parfitt, R.W.G. Grimes, J. Nucl. Mater. 381 (2008) 206.
[48] B.V. Dobrov, O.V. Khoruzhii, S.Y. Kourtchatov, V.V. Likhanskii, Nucl. Eng. Des. 195 (2000) 361.
[49] D.R. Olander, D. Wongsawaeng, J. Nucl. Mater. 354 (2006) 94.
[50] R.J. White, S.B. Fisher, P.M.A. Cook, R. Stratton, C.T. Walker, I.D. Palmer, J. Nucl. Mater. 288 (2001) 43.
[51] Y.H. Koo, B.H. Lee, J.S. Cheon, D.S. Sohn, J. Nucl. Mater. 295 (2001) 213.
[52] P. Losonen, J. Nucl. Mater. 304 (2002) 29.
[53] R.J. White, M.O. Tucker, J. Nucl. Mater. 118 (1983) 1.
[54] K. Nogita, K. Une, Nucl. Instrum. and Meth. B 141 (1998) 481.
[55] W. Smith, Mol. Simul. (2006) 933.
[56] W. Smith, I.T. Todorov, The DLPOLY 3.0 User Manual, Daresbury Laboratory, United Kingdom.
[57] K. Govers, S. Lemehov, M. Hou, M. Verwerft, J. Nucl. Mater. 366 (2007) 161.
[58] K. Govers, S. Lemehov, M. Hou, M. Verwerft, J. Nucl. Mater. 376 (2008) 66.
[59] N.D. Morelon, D. Ghaleb, J.M. Delaye, L. Van-Brutzel, Philos. Mag. 83 (2003) 1533.
[60] L. Van Brutzel, J.M. Delaye, D. Ghaleb, M. Rarivomanantsoa, J. Nucl. Mater. 83 (2003) 4083.
[61] L. Van Brutzel, M. Rarivomanantsoa, J. Nucl. Mater. 358 (2006) 209.
[62] L. Van Brutzel, M. Rarivomanantsoa, D. Ghaleb, J. Nucl. Mater. 354 (2006) 28.
[63] R.G.J. Ball, R.W. Grimes, J. Nucl. Mater. 188 (1992) 216.
[64] P.W. Tasker, J. Phys. C 12 (1979) 4977.
[65] M.R. Castell, Phys. Rev. B 68 (2003) 235411.
[66] C. Meis, A. Chartier, J. Nucl. Mater. 341 (2005) 25.
[67] J.F. Ziegler, J.P. Biersack, U. Littmark, The Stopping and Range of Ions in Solids, vol. 1, Pergamon Press, New York, 1985.